Evaluation of joint probability density function models for turbulent nonpremixed combustion with complex chemistry

By N. S. A. Smith[1], S. M. Frolov[2] AND C. T. Bowman[3]

Two types of mixing sub-models are evaluated in connection with a joint-scalar probability density function method for turbulent nonpremixed combustion. Model calculations are made and compared to simulation results for homogeneously distributed methane-air reaction zones, mixing and reacting in decaying turbulence within a two-dimensional enclosed domain. The comparison is arranged to ensure that both the simulation and model calculations a) make use of exactly the same chemical mechanism, b) do not involve non-unity Lewis number transport of species, and c) are free from radiation loss. The modified Curl mixing sub-model was found to provide superior predictive accuracy over the simple relaxation-to-mean sub-model in the case studied. Accuracy to within $10-20\%$ was found for global means of major species and temperature; however, nitric oxide prediction accuracy was lower and highly dependent on the choice of mixing sub-model. Both mixing sub-models were found to produce non-physical mixing behavior for mixture fractions removed from the immediate reaction zone. A suggestion for a further modified Curl mixing sub-model is made in connection with earlier work done in the field.

1. Introduction

A large number of practical combustion systems can be said to operate in a nonpremixed turbulent regime. Under these conditions, fuel and oxidizer react concurrently as they are mixed together through the cascade of scales from turbulent stirring down to molecular diffusion. The nonpremixed mode of combustion is distinct from the premixed mode in that the propagation of reaction fronts through a flammable mixture is not encountered. This is by virtue of the concurrence of mixing of reactants to a flammable state, and reaction.

When put in the context of the partially premixed flame studies discussed elsewhere in this volume, nonpremixed combustion refers to all the phenomena that occurs after the passage of any initial igniting flame fronts. The bulk of chemical activity in gas turbine combustors, compression ignition internal combustion engines, and a great many other classes of devices, occurs downstream of stabilizing flow structures in a purely nonpremixed mode.

1 Center for Turbulence Research
2 N. N. Semenov Institute for Chemical Physics, Moscow, Russia
3 Stanford University

The critical design issues facing gas turbine combustor and diesel engine designers at present center on reducing pollutant formation in order to meet present and future emission regulations. In order to understand and be able to predict the occurrence of unwanted byproducts, such as oxides of nitrogen (NO_x) and soot, it is essential that allowances be made for the interactions which occur between finite rate chemical reactions and turbulent mixing processes. Nitric oxide (NO) is a species whose formation in flames is limited by chemical kinetic rates which are slow in comparison to typical mixing rates, and thus cannot be adequately predicted using a model assumption of mixing-limited chemistry.

Many methods have been proposed which seek to accurately predict the interaction of finite rate chemistry and turbulent mixing. One of the most promising groups is the Joint Probability Density Function (JPDF) methods as employed by Pope (1981, 1985, 1990) and others (see Chen & Kollmann 1988, 1992, 1994). The variants of the JPDF method have been used to successfully predict nitric oxide formation in turbulent jet diffusion flames of hydrogen (Chen & Kollmann 1992, Chen *et al.* 1995, Smith *et al.* 1993). The effectiveness of the JPDF model in these experimental comparisons for hydrogen and other tests involving hydrocarbon fuels (Chen 1996) make it a prime candidate for incorporation in design tools for use with more practical combustion systems.

Correa and Pope (1992) have already begun to take steps towards implementing JPDF methods in a computational framework more suited to practical calculations. They showed reasonable agreement between the predictions of a hybrid JPDF method in an elliptic flow solver, with experimental data gathered behind a bluff body stabilized flame. One difficulty with the experimental comparison of Correa and Pope (1992) and those of the jet flame experiments described above is that there are a number of other models and approximations that must be incorporated in order to produce useful predictions, but these other models make it difficult to ascertain the inherent accuracy of the JPDF method.

Where only a *scalar* JPDF method is employed (as in the studies cited), a turbulence model must be used to solve for the turbulent flow field. In the jet flame studies, radiation modeling can be problematic (Smith *et al.* 1993, 1996) and thus make it difficult to evaluate the performance of the JPDF model directly. Further, since the JPDF model cannot be easily employed with large chemical reaction mechanisms, due to computational constraints, it is often necessary to employ reduced chemical descriptions of the full reaction set. This modeled abbreviation of a chemical system also introduces uncertainty when comparing with physical experiments.

Extraneous modeling issues can be swept aside if direct numerical simulation (DNS) is used as an evaluation tool. With DNS it is possible to construct an idealized numerical experiment where unwanted physical effects can be excluded by design. For the case of mixing and reaction of fuel and oxidizer pockets in decaying isotropic turbulence, the flow field is at its simplest, radiation losses can be dropped from consideration, and commonality between the modeled and simulated chemical reaction schemes can be ensured.

The purpose of this study was to compare JPDF model predictions with DNS

observations for the nonpremixed combustion of methane and air in decaying turbulence. The chemical mechanism employed in both the DNS and in the JPDF model calculations included prompt and thermal NO formation pathways and so allowed an evaluation of the model's NO prediction capabilities to be made.

2. Joint scalar PDF equations

Given a chemical system of N species it is possible to construct a chemical composition vector, where each coordinate corresponds to a possible species mass fraction. It is then possible to define the probability F that the instantaneous composition vector at a time t at a sample point is in the immediate vicinity of $\underline{\psi}$.

$$F(\psi_1, \ldots, \psi_N; t) \equiv Prob\{\psi_1 < \phi_1 \leq \psi_1 + d\psi_1, \ldots, \psi_N < \phi_N \leq \psi_N + d\psi_N\} \quad (1)$$

The density-weighted joint scalar probability density function, $\tilde{f}$, in composition space is then defined as the partial derivative with respect to the species dimensions.

$$\tilde{f}(\psi_1, \ldots, \psi_N) \equiv \frac{\rho(\psi_1, \ldots, \psi_N)}{<\rho>} \frac{\partial^n F}{\partial\phi_1 \ldots \partial\phi_N} \quad (2)$$

For homogeneous flows, the evolution of the joint scalar PDF is then given by the following (see Chen and Kollmann 1994), where $\dot{Q}_k$ is the instantaneous reaction rate of the kth species at time t, and $\chi_{k,l}$ is the joint scalar dissipation rate for the kth and lth species.

$$\frac{\partial \tilde{f}}{\partial t} + \frac{\partial}{\partial \phi_k}(\dot{Q}_k \tilde{f}) = -\frac{\partial^2}{\partial\phi_k \partial\phi_l}(\chi_{k,l}\tilde{f}) \quad (3)$$

The influence of chemical reactions on the temporal evolution of the joint scalar PDF is similar to a convective velocity field in composition space. Dissipation of scalar fluctuations through mixing, as represented by the second right hand side term, lead to reductions in the variances and covariances of the species and a sharpening of the joint PDF at the mean composition.

As chemical systems of practical interest can have an extremely large number of important species, the dimensionality of the joint PDF can also be large. Stochastic methods recommend themselves as the solution method of choice in these cases (Pope 1981).

In a Monte Carlo approach, a large number of stochastic particles are operated upon by model processes in a Lagrangian frame of reference. The model processes are designed in such a way as to cause the joint PDF of all the particles to behave according to the evolution equation above.

Each stochastic particle has a definite location in composition space at any given time. The evolution of the ith chemical component of the jth stochastic particle can be expressed in terms of a chemical reaction source term, $\dot{Q}_i^j$, and molecular mixing term, $\dot{m}_i^j$, as given below.

$$\frac{\partial \phi_i^j}{\partial t} = \dot{Q}_i^j + \dot{m}_i^j \tag{4}$$

A significant advantage of the JPDF method over other models is that the chemical source terms $\dot{Q}_i^j$ can be evaluated exactly without need for a model. The difficulty with the Lagrangian formulation lies with the treatment of the molecular mixing terms $\dot{m}_j^i$.

2.1 Molecular mixing models

A wide variety of molecular mixing models have been proposed for $\dot{m}_i^j$ in the past (see Pope 1981, Chen and Kollmann 1994). The simplest useful model is a deterministic relaxation-to-the-mean (RTM) expression as given below, where ω denotes a turbulent mixing frequency.

$$\dot{m}_i^j \approx \omega(< \phi_i > - \phi_i^j) \tag{5}$$

The deterministic RTM model has the advantage of being simple to implement within a complex practical calculation and allows the mixing and reaction terms of the stochastic equations to be solved simultaneously. All particles are operated on by both the molecular mixing and reaction models at all stages of the computation. A disadvantage of the RTM model is that it does not predict the correct mixing behavior of two fluids in an isotropically decaying turbulent field. Instead of causing a mixture fraction PDF to tend towards a Gaussian distribution with increasing time, the RTM model allows the flatness of the PDF to increase without bound.

More sophisticated mixing models have been derived from the Curl coalescence-dispersion models for droplet mixing. Whereas the original Curl mixing model gives rise to discontinuous joint PDFs, the modified Curl model proposed by Janicka *et al.* (1979), and Dopazo (1979), yields the desired continuous joint PDFs. Mixing is modeled by operating on a small number of particles at each time step of the calculation. Particle pairs are chosen at random from the complete particle ensemble, and are caused to mix with one another to a randomly varying degree α. The resultant compositions of the jth and kth particle after mixing interaction are given by the following.

$$\phi_i^{j*} = \alpha \phi_i^j + \frac{1}{2}(1-\alpha)(\phi_i^k + \phi_i^j) \tag{6}$$

$$\phi_i^{k*} = \alpha \phi_i^k + \frac{1}{2}(1-\alpha)(\phi_i^k + \phi_i^j) \tag{7}$$

The number of random particle pair selections that must be made per timestep of the calculation is given by the following (see Pope 1982), where B is a constant number that depends on the pair selection scheme, and $\omega \delta t$ is the timestep nondimensionalized by the mixing frequency.

$$N_{pairs} = B \omega \delta t N_{particles} \tag{8}$$

The use of random particle interaction (RPI) models provides a framework for the implementation of schemes that reflect more of the physical nature of mixing. An example of the benefit that can be derived from RPI models can be found in the "particle age" modification suggested by Pope (1982). This model can be tuned to enforce asymptotic Gaussianity on conserved scalar PDFs in decaying isotropic turbulence.

One potential drawback incurred in using particle interaction models is that the mixing process can then no longer be solved simultaneously with the chemical reaction process. The two processes must be decoupled, and this can cause problems where the rates of mixing and reaction are both very large relative to the inverse of the timestep. Such problems are likely to occur when combustion occurs in the flamelet regime (see Anand & Pope 1987).

Both the RPI model and the simple RTM model were employed in JPDF calculations against the DNS data. The results of this comparison are presented in Section 4.

3. Simulation conditions

Due to resource and time constraints, the direct numerical simulation was limited to a two-dimensional calculation of nonpremixed combustion in a decaying turbulent field.

As the JPDF method is inherently statistical in nature, it was desirable to maximize the number of DNS data points in the domain that could be included in a single statistical set. To this end, the simulation was performed with an initially isotropic turbulent velocity field and distribution of fuel and oxidizer pockets. The initial distribution of chemical species was determined from a phase scrambled E^{-k} spectrum for a conserved scalar, known as mixture fraction ξ (see Fig. 1).

Mixture fraction is a normalized scalar that is equal to unity where all of the local has mass originated from the nominal fuel source, irrespective of its reacted state, and zero where all the local mass has originated from the oxidizer source.

Given the distribution of the conserved scalar, mixture fraction (ξ), reactive scalar profiles were mapped onto the domain according to adiabatic equilibrium profiles in mixture fraction space (see Fig. 2).

Zones on the domain with a stoichiometric mixture fraction ($\xi = 0.055$) were thus assigned a species and temperature composition corresponding to adiabatic equilibrium conditions at stoichiometric. Domain regions with higher or lower mixture fraction values were given correspondingly richer or leaner blends of equilibrated fluid.

Note that the richest mixture fraction allowed in the initialization of the simulation domain was $< \xi >= 0.15$. This mixture fraction is beyond the rich flammability limit of methane-air mixtures at standard temperature and pressure. Of all the species present in the simulation, only nitric oxide (NO) was initialized as being zero at all mixture fractions.

By initializing the simulation using the method described above, the flame zones were effectively ignited simultaneously, albeit artificially, prior to run time. This

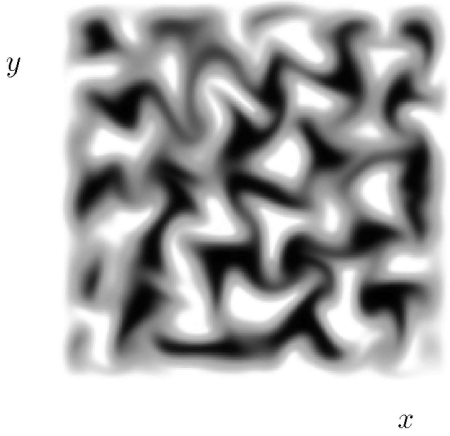

FIGURE 1. Initial distribution of the conserved scalar. Dark regions denote fuel rich zones $\xi = 1$ while light regions denote fuel lean zones $\xi = 0$.

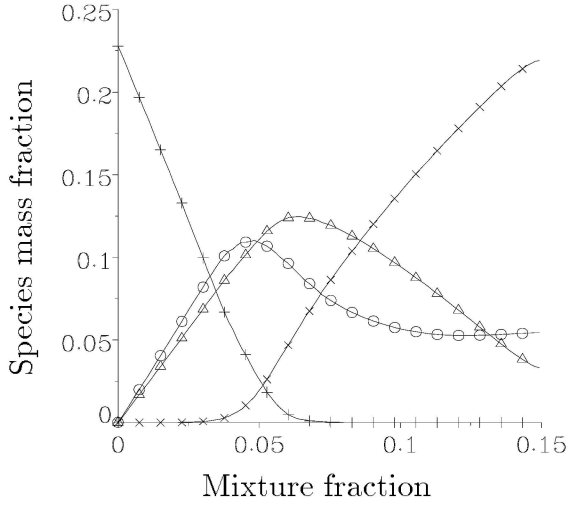

FIGURE 2. Adiabatic equilibrium species mass fraction profiles in mixture fraction space. Symbol key : $+$ - O_2, $\times$ - CO, $\circ$ - CO_2, $\triangle$ - H_2O.

was done to avoid a potentially long transient period where (presumably) triple flames would propagate along the unburnt flammable ribbons between the fuel and oxidizer pockets away from the ignition points.

In order to avoid the establishment of intense pressure waves as a result of mapping flame zone temperatures onto an initial cold flow field, the local densities were adjusted everywhere to maintain a uniform initial pressure field. The existence of large density gradients after initialization caused a short period where the flow field reorganized to preserve continuity. It is difficult to draw a parallel in behavior between the decay of turbulent motions in the reacting case and the well known trends in inert grid turbulence. The former case is subject to dilatation, variable

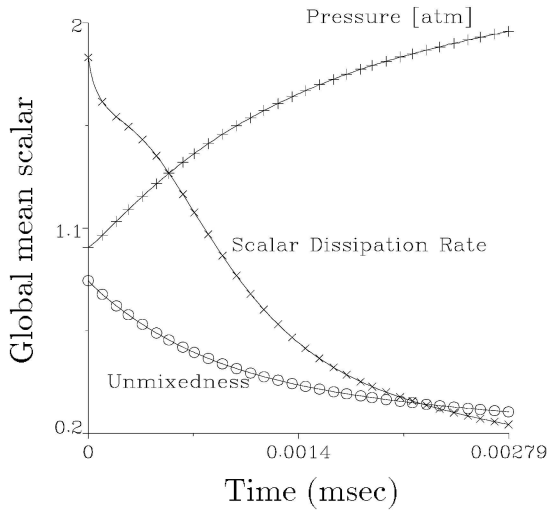

FIGURE 3. Variation in simulated global mean quantities with calculation time.

viscosity, and baroclinic torque effects that are absent in the latter.

Unfortunately, it was further found that it was not possible to perform simulations with a combination of periodic boundary conditions and the initialization technique described above. No satisfactory explanation for this restriction has been found. It was found, however, that the calculation could proceed without hindrance if the domain was instead bounded by adiabatic slip walls encompassing a small filter zone with initially damped wall-normal velocity.

Under the simulation conditions described above, the flow and mixing fields on a central portion of the grid (210^2) were found to be statistically homogeneous. All of these points were then used in each of the statistical samples taken periodically throughout the temporal evolution of the simulation. With the passage of time, turbulent motions caused parcels of fuel and oxidizer to be convected into close proximity while molecular diffusion fed the reaction zones present at the fuel/oxidizer interfaces.

Unmixedness, U, is defined here as the global variance of mixture fraction normalized by the maximum possible variance, which is given by the product of the differences between the global mean and the maximum and minimum possible values of conserved scalar. Unmixedness is thus equal to unity when no mixed fluid is present, and zero when all fluid has been mixed to a uniform state. The gradual decay in the unmixedness of the conserved scalar is plotted along with nondimensional scalar dissipation rate and mean pressure in Fig. 3.

It is evident that the molecular mixing processes promoted by turbulent stirring rapidly mixed the conserved scalar towards uniformity, but that at the end of the simulation the unmixedness was still substantial at approximately $U = 0.3$. As a result of the increase in the characteristic turbulent time scale and the decrease in local conserved scalar gradients, the scalar dissipation rate can be seen to decrease with time.

The simulation was carried out using a Fickian assumption for the molecular

transport of the species, as traces, in a background gas (N_2). All species were assigned uniform Lewis numbers of unity in order to allow a fair comparison with the JPDF model predictions. The JPDF model is not strictly valid where significant differential molecular diffusion between the species is present.

As the reactions proceeded, more and more fuel and oxidizer were consumed and progressively more sensible enthalpy was released into the system. The release of heat in the confined system caused the mean pressure in the domain to double over the course of the simulation (see Fig. 3). The change in global mean species mass fractions during the course of the simulation can be seen in Fig. 4.

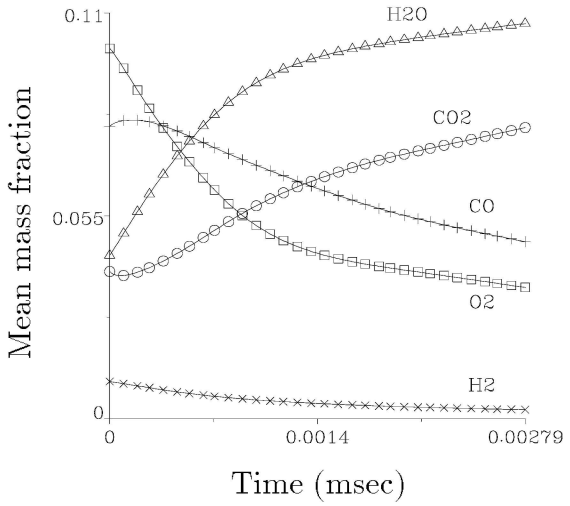

FIGURE 4. Variation in simulated global mean species mass fractions with calculation time.

The turbulent Reynolds number determined use of the mean molecular viscosity (recall that the local temperature variations give rise to a seven-fold variation in local dynamic viscosity) slowly from approximately 30 down to 20 over the duration of the simulation.

The simulation conditions correspond physically to a small area of intensely mixed fluid of the order of 3 millimeters on each side. In some ways the simulation conditions may be analogous to the kind of conditions experienced inside high power-density combustion devices of practical interest. The DNS domain might be thought of as representing a single computational cell in a much larger grid used in a practical model calculation. In this sense it is of some interest to observe how well the JPDF model performs in this single cell, as it could well have implications for use of the model in a large multi-cellular calculation.

With the assumption of isotropy, the JPDF model reduces to a dimensionally degenerate case devoid of mean gradients. The case is similar to those studied by Correa (1993) and Chen (1993), except that it is unsteady, whereas the earlier studies were for steady combustion.

3.1 Chemical reaction mechanism

An eight step reduced chemical mechanism for methane combustion was provided by Frolov (1996) for use in both the DNS and JPDF calculations. The mechanism consists of global steps which do not make explicit use of any radical species, such as hydroxyl (OH), methyl (CH_3), and so on, but instead employs tuning factors for the fuel oxidation and prompt NO_x steps. These tuning factors are incorporated into the pre-exponential coefficients in the Arrhenius expressions and make allowance for variations in local equivalence ratio, fuel species, and pressure. The tuning constants were derived by Frolov (1996) from comparison of the reduced mechanism with full mechanism calculations in counterflow laminar premixed flames.

$$CH_4 + 1.5O_2 \rightarrow CO + 2H_2O \qquad (I)$$

$$CO + H_2O \rightarrow CO_2 + H_2 \qquad (IIf)$$

$$CO_2 + H_2 \rightarrow CO + H_2O \qquad (IIb)$$

$$2H_2 + O_2 \rightarrow 2H_2O \qquad (III)$$

$$2CO + O_2 \rightarrow 2CO_2 \qquad (IV)$$

$$CH_4 + O_2 + N_2 \rightarrow CH_4 + 2NO \qquad (V)$$

$$N_2 + O_2 \rightarrow 2NO \qquad (VIf)$$

$$NO + NO \rightarrow N_2 + O_2 \qquad (VIb)$$

The Arrhenius rate constants corresponding to the above reaction steps are given below where A_i, n_i and E_i denote the pre-exponential factor, temperature index, and activation energy for reaction number i, and p is the local pressure in bar.

No.	$A_i(mol, L, s)$	n_i	$E_i(kcal/mol)$
I	A_1/p	0.0	50.0
IIf	$1.0 \times 10^{12}/p$	0.0	41.5
IIb	$3.1 \times 10^{13}/p$	0.0	49.1
III	$7.0 \times 10^{13}/p^2$	0.0	21.0
IV	$8.5 \times 10^{12}/p^2$	0.0	21.0
V	A_5/p^2	0.0	50.0
VIf	1.7×10^{17}	-0.5	136.0
VIb	4.1×10^{15}	-0.5	93.3

The pre-exponential factors for reactions I and V are functions of the local equivalence ratio β. Frolov (1996) determined the appropriate values of A_1 and A_5 at a range of equivalence ratios from $\beta = 0.67$ up to $\beta = 1.54$. The pre-exponential factors vary nonlinearly over the range such that the lean limit values are orders of magnitude greater than the rich limit values. The values under stoichiometric conditions for each is $A_1 = 2.57 \times 10^{15} L/(mol \cdot s)$ and $A_5 = 7.03 \times 10^{13} L^2/(mol^2 s)$.

At the suggestion of Frolov (1996), linear interpolation between the known values for A_1 and A_5 was used to determine values for intermediate mixing states.

At this stage there are some questions as to the accuracy of the chemical mechanism described above, since it appears to give quantitatively inaccurate values for unstrained laminar flame speed and extinction strain rate. However, as both the DNS and JPDF computations employed the same chemical mechanism, the quantitative accuracy of the mechanism is not an issue in comparing one with the other.

4. Comparison of predictions and simulation data

The JPDF model calculations were in each case initialized directly from the domain of the DNS data base. Each of the 2,000 stochastic particles used in the model were assigned compositions selected at random from the domain. Special care was taken to ensure that the initial particle distribution in composition space gave rise to the same statistics as was found in the simulation. As the particles used in the model were of equal mass, this required that the number of potential particle assignments for each domain cell be proportional to the local fluid density.

An assignment table was constructed for the purpose of particle initialization, where there was an equal probability of a particle being assigned the composition of any entry in the table. The number and composition of the table entries was determined from the simulation domain, such that a very low density cell would only provide a single entry whereas a high density cell would provide a number of repeated entries, each with the same composition as the originating cell. As the central portion of the simulation domain consisted of approximately 45,000 cells and the ratio of the mean cell density to the minimum cell density was of order $2-3$, this gave rise to a table containing around 100,000 entries. Of that number, 2,000 were selected at random, without replacement, for particle assignment.

Model calculations were then allowed to proceed according to Eq. 3, with a revised mean pressure calculated after every time step. Mixing time scales were drawn from the DNS for use in the model calculation.

4.1 Global mean behavior

Global mean species yields and pressure were predicted using RTM and RPI mixing sub-models (see Section 2.1) within the JPDF model.

Typical model predictions for mean pressure, initialized from the initial DNS data, are plotted in comparison with the DNS pressure record in Fig. 5. The RTM prediction displays too slow an initial pressure rise, indicating a too modest sensible energy release rate. Towards the end of the simulation period, the RTM-modeled mean pressure rises at a rate greater than that seen in the DNS.

The random particle interaction model prediction tends to lie substantially closer to the DNS curve than do the predictions of the RTM model. At its worst the RTM model exhibits an approximate 20% discrepancy below the DNS curve, while the RPI model exhibits a maximum underprediction on the order of 10%.

The model predictions for mean carbon dioxide (CO_2) mass fraction formation reflect the predicted mean pressure behavior (see Fig. 6). Carbon dioxide is one of

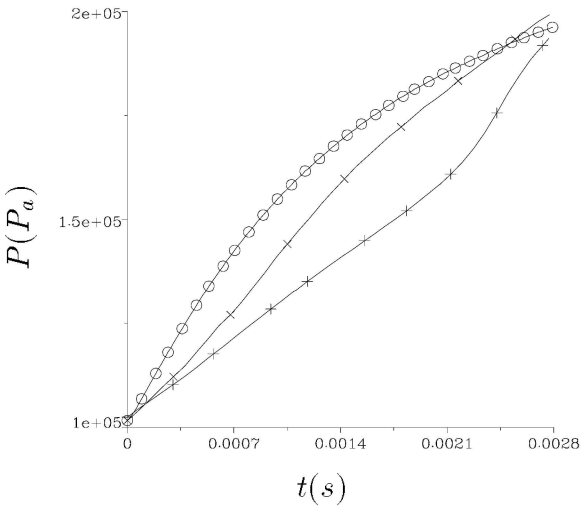

FIGURE 5. Comparison of simulated and predicted mean pressure rise. chemical description of H_2/N_2-air combustion. Symbol key : + - JPDF-RTM, × - JPDF-RPI, ○ - DNS.

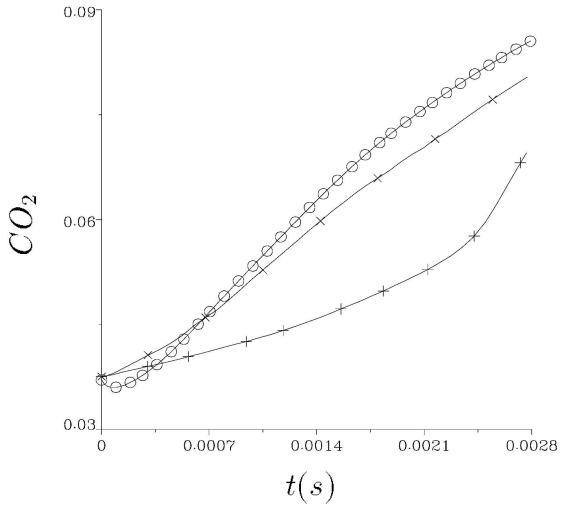

FIGURE 6. Comparison of simulated and predicted overall mean CO_2 production. Symbol key : + - JPDF-RTM, × - JPDF-RPI, ○ - DNS.

the principal exothermic products of hydrocarbon combustion, with the release of sensible energy being closely linked to its oxidation from carbon monoxide (CO).

The carbon dioxide mass fraction curve predicted by the RTM mixing model displays the same tendency as the corresponding mean pressure curve. The initial formation of CO_2 proceeds at a slow rate before sharply increasing towards the end of the simulation.

As was the case for the mean pressure, the RPI prediction for CO_2 formation does not display this kind of sharp increase. Instead the curve has the same kind of gradual decrease in slope that can be seen in the simulation data.

Carbon monoxide (CO) is in great abundance at the beginning of the simulation, having been initialized using adiabatic equilibrium values at each value of mixture fraction. These equilibrium values are not normally encountered in flames since any substantial level of molecular transport tends to move CO into reaction zones at leaner mixture fractions, where it is consumed.

As a result of the initially high levels of CO, it acts primarily as a fuel species in the simulation. It is oxidized to form CO_2, releasing heat in the process. Typical predicted mean mass fraction curves for carbon monoxide are compared with the simulation in Fig. 7. It is again evident that the JPDF model using the RTM mixing sub-model tends to underpredict the initial reaction rate, but displays a sharp increase in reactant consumption towards the end of the simulation.

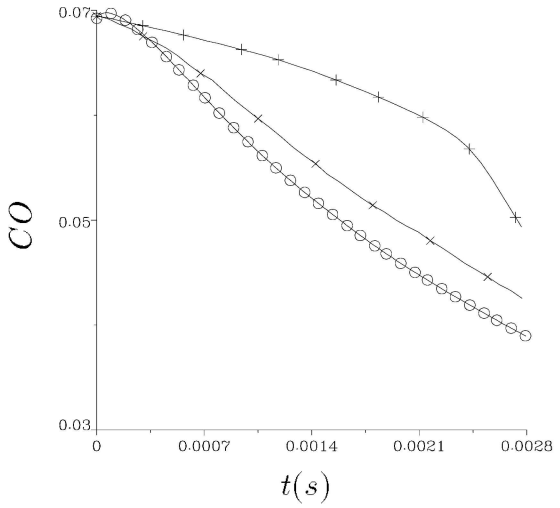

FIGURE 7. Comparison of simulated and predicted global mean CO consumption. Symbol key : + - JPDF-RTM, × - JPDF-RPI, ○ - DNS.

The prediction of nitric oxide (NO) formation is particularly difficult given its high sensitivity to local temperature and oxygen concentration. The equilibrium concentration for NO under hot combusting conditions is orders of magnitude greater than what is usually observed in practice. Unlike the major species, the formation of NO is limited not by the rate of mixing but by the chemical kinetic rate at which mixed species will react.

Typical JPDF model predictions for mean nitric oxide mass fraction, derived using RTM and RPI mixing submodels, are compared with simulation data in Fig. 8. The profiles from all three sources exhibit increases with time, which indicates the level of NO is far below its equilibrium condition. The second derivative with respect to time of all three profiles is positive over the course of the simulation.

The significance of small differences in model assumptions on NO prediction is highlighted by the fact that the RTM and RPI curves straddle the observed DNS curve. The nitric oxide formation rate predicted by the RTM submodel is substantially less than the simulated rate, whereas the RPI predicted rate is somewhat greater.

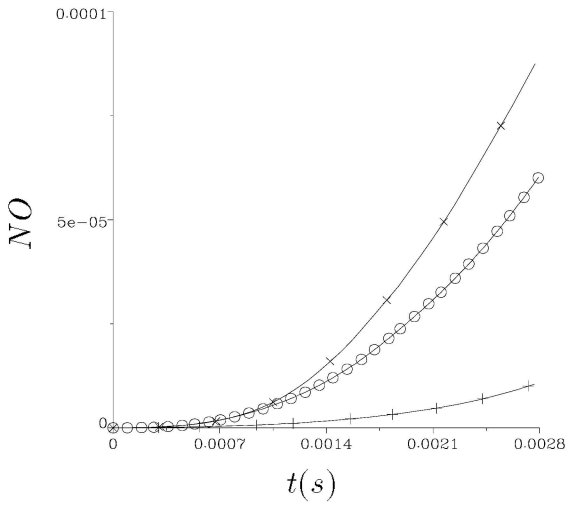

FIGURE 8. Comparison of simulated and predicted global mean NO formation. Symbol key : + - JPDF-RTM, × - JPDF-RPI, ○ - DNS.

4.2 Behavior in mixture fraction space

The comparison of global mean statistics presented above indicates that substantial differences in model predictions arise from the choice of mixing submodel.

The characteristic differences that arise due to the choice of mixing model can be seen in Fig. 9, which depicts a typical comparison of the instantaneous scatter of stochastic particles in mixture fraction and CO_2 mass fraction space. The comparison of particle scatter is made at the end of the calculation ($t = 2.80ms$), bearing in mind that the particle scatter was identical at $t = 0$.

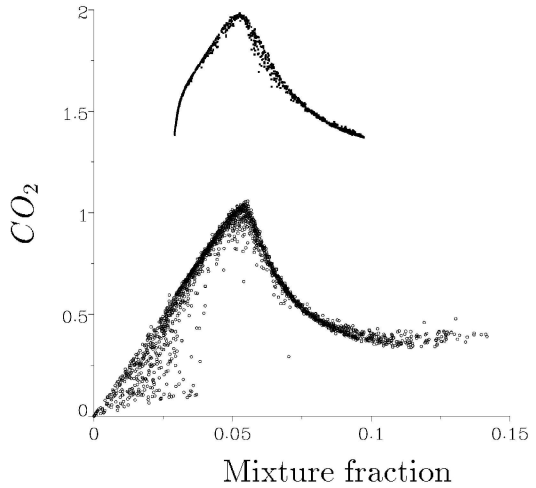

FIGURE 9. Comparison of predicted CO_2-mixture fraction distribution of stochastic particles at time $t = 2.80ms$. The RTM (upper) profile has been uniformly shifted by an offset in CO_2 mass fraction of 1.0 for the sake of clarity. The RPI (lower) profile is unshifted.

Despite the fact that both distributions have the same overall mixture fraction mean and variance, the range in particle values is much greater in the case of the RPI-modeled distribution. This is because, in contrast to RTM where all particles mix at every step, the RPI model only mixes a relatively small random selection to a potentially large degree. The random nature of the RPI mixing model allows unselected particles to remain far from the mean of the distribution. As a result, the kurtosis of the RPI-predicted mixture fraction distribution tends to be higher than that predicted by the RTM model, and for that matter the DNS data (not shown).

In addition, the qualitative forms of the two distributions are quite different. The RTM-predicted distribution exhibits far less scatter than its RPI-predicted counterpart at any given mixture fraction. This is because in the RTM model, all particles relax towards the mean position in composition space at a rate which depends only on the mixing frequency (same for all particles) and the distance between the particle and the mean position. Thus two particles that are initially very close together will both proceed towards the global mean composition, though they will never interact. In the absence of chemical reactions, the RTM mixing model causes the initial profile to contract with time in a self-similar fashion towards the mean position. Thus the distribution plotted in Fig. 9 is virtually a contracted image of the initial particle distribution, albeit somewhat perturbed by chemical reactions.

This self-similar behavior is in contrast to the RPI model where particle-to-particle interactions are what drive the overall distribution towards the mean position in composition space. Unlike with the RTM process, two particles which are initially very close in composition space may diverge substantially during the course of a single mixing step, as a result of random interaction with other particles. Conversely, two particles which are in close proximity in mixture fraction space may have widely different reactive species compositions as a result of their different individual time histories.

This is not possible under the RTM mixing model where nearby particles automatically have very similar time histories. The trajectories of all particles through composition space are constrained to approach the overall mean.

Under RPI, differences in particular reactive species compositions will be most pronounced in zones where the reaction rates pertaining to the particular species are slow compared to mixing rates. In the case of carbon dioxide (Fig. 9), scatter is greatest at mixture fractions corresponding to very rich and very lean stoichiometries where the CO_2-influencing reactions are comparatively weak.

The degree of freedom of movement of particles through composition space has implications for the accurate prediction of reactive species yields. Due to the non-linear nature of non-isothermal chemical reactions, small fluctuations in local temperature and species concentrations can lead to large changes in the production rates of species and sensible energy. These changes in kinetic rates then have an impact on the mean behavior of the system through mixing.

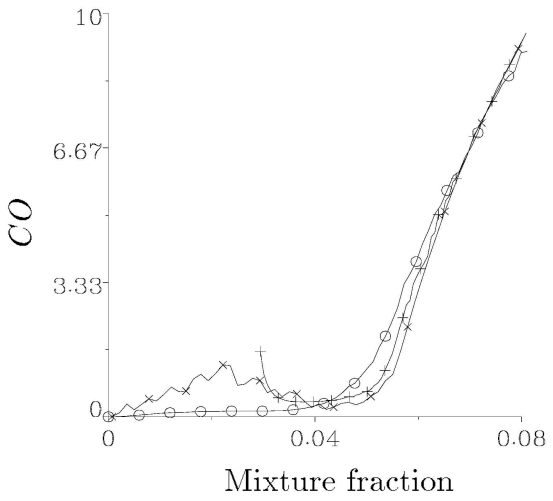

FIGURE 10. Comparison of predicted conditional mean normalized CO mass fraction profiles at time $t = 2.80ms$. Symbol key : + - JPDF-RTM, × - JPDF-RPI, ○ - DNS.

4.2.1 Conditionally averaged statistics

Conditional statistics were determined from both the predicted and simulated data by subdividing mixture fraction space into one hundred bins of equal width. Conditional means and root mean square deviations were computed within each bin for each data set at various calculation times.

The general behavior of the conditional mean profiles drawn from the simulation is one of a slow relaxation towards chemical equilibrium at an elevated pressure, after a rapid perturbation from the initial condition. The initial perturbation of the system resulted from the relatively strong mixing processes at the beginning of simulation which served to transport reactive scalars rapidly through mixture fraction space. As the level of turbulent mixing decayed with time, the degree of scalar transport decreased, thereby allowing the chemical system to return towards chemical equilibrium.

Characteristic trends in a return towards chemical equilibrium, (see Barlow *et al.* 1989, 1990) include upward relaxation in the conditional mean profiles for major product species (CO_2, H_2O) and temperature around stoichiometric. There is also a corresponding downward relaxation in fuel and oxidizer levels. Nitric oxide levels at stoichiometric increase rapidly, having been orders of magnitude below chemical equilibrium at the time of initialization.

Shortcomings in the current particle mixing models are apparent when predicted conditional mean profiles are compared with the simulation. The profiles for CO (normalized by the initial adiabatic equilibrium value at stoichiometric) at time $t = 2.80ms$ are plotted in Fig. 10. The elevated levels of CO at lean mixture fractions on the part of the models are anomalous and are not present in the simulation. The degree of this lean profile elevation decreases with increasing computation time, as the intensity of the turbulent mixing decreases.

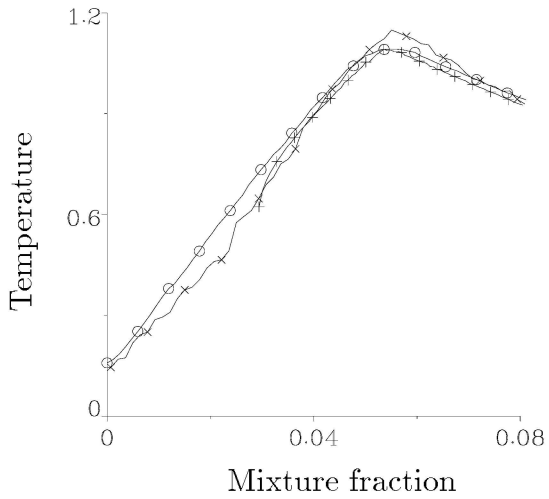

FIGURE 11. Comparison of predicted conditional mean normalized temperature profiles at time $t = 2.80ms$. Symbol key : + - JPDF-RTM, $\times$ - JPDF-RPI, $\circ$ - DNS.

The equations for the diffusive transport of reactive scalar mass fractions in mixture fraction space (see Klimenko 1990) indicate that the negative curvature of the conditional mean CO profile in mixture fraction space must result in a local decrease in the CO mass fraction profile. Similarly, chemical reactions should drive conditional mean CO levels downward. There is no obvious *physical* explanation as to how the observed elevated profiles could have been produced from the initial condition.

A similar anomalous effect can be seen in the normalized conditional mean temperature profiles in Fig. 11, where the modeled mixing processes have caused the lean portion of the temperature profile to be depressed below the expected equilibrium line. The temperature depression is more substantial at earlier times and seems to be responsible for the early underprediction of mean pressure rise seen in Fig. 5.

It is evident that the profile deviations are due to shortcomings in both the RPI and RTM mixing models. In effect, the models allow particles to mix towards a mean position that can be very far from their local region of composition space. Thus, in the case of the RPI model, particles at very lean mixture fractions are just as likely to mix with other particles at very rich mixture fractions as those immediately adjacent to themselves. The RTM model effectively allows the same interaction by constraining particles to mix along trajectories towards the overall mean position.

In reality, a fluid parcel is not free to mix with any other fluid parcel; it is instead bound to interact with those in its immediate vicinity in composition space. Parcels in a fluid continuum cannot *jump* between separated locations in composition space, given a certain time step, without having an impact upon the intervening compositions. In the case of the conditional mean CO profile of Fig. 10, the elevated levels on the lean side of the reaction zone can only exist if the CO values at stoichiometric

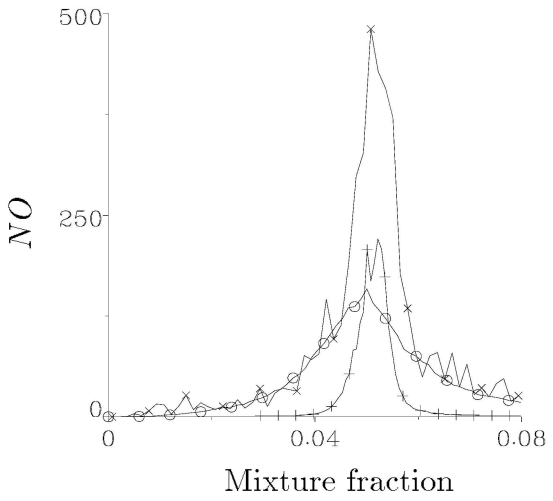

FIGURE 12. Comparison of predicted conditional mean NO mass fraction [ppm] profiles at time $t = 2.80ms$. Symbol key : + - JPDF-RTM, $\times$ - JPDF-RPI, $\circ$ - DNS.

are more elevated still. There is no possibility of counter-gradient transport in the simulation given the assumptions employed.

Turning to the prediction of nitric oxide (NO) formation, a comparison of conditional mean profiles from the models and the simulation can be made from Fig. 12. It is clear that in all cases the formation of NO is strongly centered on the high temperature reaction zones around stoichiometric. Of the two predictions, those of the RPI model seem to best match the simulation profile at lean and rich mixture fractions in capturing the transport of NO to inert zones in mixture fraction space.

An explanation for the significant discrepancy between the two model predictions for NO can be found in the difference between the conditional mean and variance profiles of temperature. Throughout the calculations, the particles in the vicinity of the reaction zone have a slightly higher conditional mean temperature under the RPI model than the RTM model. Further, the level of conditional variance in the temperature under the RPI model is many times greater than what is observed under the RTM model.

The RPI model predicts a slightly higher conditional temperature variance than the simulation, around stoichiometric, while having conditional mean temperature values similar to the prediction. Given the high nonlinear sensitivity of NO formation to temperature, it is reasonable to speculate that this difference in conditional variance may be the cause of the observed NO discrepancy.

5. Discussion

It is reasonable to assert that the RPI mixing model as described above seems to perform better than the RTM mixing model under the conditions examined. The overall prediction of mean species yields by the RPI-JPDF combination is superior to that seen for the RTM-JPDF combination in the tests conducted.

The RPI model seems to incorporate significant conditional root mean square deviations in reactive species levels in mixture fraction space. This in turn may allow better prediction the formation of thermochemically sensitive species such as NO. Indeed, in cases where highly nonlinear phenomena such as extinction behavior is to be predicted, the RTM approach would be unable to capture the significant contributions made by particles that are far from the conditional mean profiles.

Both models, however, seem to suffer from a "long range mixing" problem. That is to say that particles are allowed to freely mix with other particles that are far removed in mixture fraction space, without having any effect at all on particles that lie in the intervening space.

The Kolmogorov *scalar* scale (η_k), defined below (where τ_k is the Kolmogorov time scale, and χ is the mean scalar dissipation rate), describes the characteristic fluctuations in a conserved scalar which are present at the smallest eddy sizes, i.e. the level of scalar fluctuations which are diminished by molecular diffusion alone.

$$\eta_k \equiv (\chi \tau_k)^{1/2} \tag{9}$$

After making an assumption about the relationship between the scalar dissipation rate, the scalar variance, and the turbulent time scale, it is possible to express η_k approximately as given below.

$$\eta_k \propto < \xi'^2 >^{1/2} / Re_t^{1/4} \tag{10}$$

As the turbulent Reynolds number (Re_t) in the simulation performed in this study was rather low, the Kolmogorov scalar scale was on the order of one fifth of the entire range of mixture fraction space. In practical turbulent reactors, one might expect this value to be substantially lower.

Using the Kolmogorov scalar scale as a guide for the case studied here, it seems unlikely that any particle would be able to mix on a molecular level with any other particle that is any further than $\Delta\eta = 0.03$ distant.

It may be appropriate to attempt to modify the RPI mixing model presented here so as to limit the range in mixture fraction space over which particles are allowed to interact. In so doing, a greater number of particle interactions would be required in each time step so as to correctly model the overall decay rate in mixture fraction variance.

Chen and Kollmann (1994) suggest a modified RPI model which better represents molecular diffusion by limiting the range over which particles can interact. No mention of a criteria for this critical range was mentioned, but perhaps the Kolmogorov scalar scale could be used in this capacity. To the best of the authors' knowledge, this scheme has yet to be implemented for testing.

6. Comments

This preliminary work has served to illustrate the effective differences between different mixing sub-models employed in a scalar JPDF model for nonpremixed turbulent combustion.

The simulation conditions were admittedly difficult to model, given that the non-premixed reaction zones were initially quite thin compared to both the physical and mixture fraction scales of the domain. Nevertheless, practical multi-cellular calculations using JPDF methods will likely involve discretizations with cell Reynolds and Damköhler numbers of the same order as that encountered in the simulation. In that regard, the insight obtained here could be of some use in selecting a mixing sub-model for practical usage.

It would seem that of the two mixing sub-models tested, the Random-Particle-Interaction (RPI) model proved both to be more accurate in prediction, and also to exhibit more of the qualitative characteristics of the mixing processes observed in the simulation. Both mixing sub-models were found to exhibit non-physical behavior in the sense that particles were free to interact over too wide a range in mixture fraction space.

The RPI model seems to be best suited for modification to include some limitation on mixing interaction distances in mixture fraction space. The implementation and testing of this modification as described in the discussion and by Chen and Kollmann (1994) is a project for future work in this area.

Further, as computational resources become available it would be valuable to simulate a three dimensional case of the conditions studied here. This would be done to determine if important effects have been neglected in the current simulation and would have the advantage of carrying a much larger number of statistical sample points in the analysis.

REFERENCES

Anand, M. S., & Pope, S. B. 1987 Calculations of premixed turbulent flames by pdf methods. *Combust. Flame.* **67,** 127-142.

Barlow, R. S., Dibble R. W., & Fourgette D. C. 1989 *Departure from chemical equilibrium in a lifted hydrogen flame.* Sandia Report SAND89-8627.

Barlow, R. S., Dibble, R. W., Chen, J.-Y., & Lucht, R. P. 1990 Effect of Damköhler number on super-equilibrium OH concentration in turbulent non-premixed jet flames.. *Combust. Flame.* **82,** 235.

Chen, J.-Y. 1993 Stochastic Modeling of Partially Stirred Reactors. Presented at the Fall Meeting of the Western States Section of the Combustion Institute. Menlo Park, California.

Chen, J.-Y. 1996 Private communication.

Chen, J.-Y., Chang, W.-C., & Koszykowski, M. L. 1995 Numerical Simulation and Scaling of NOx Emissions from Turbulent Hydrogen Jet Flames with Various Amounts of Helium Dilution. *Combust. Sci. Tech.* **110,** 505.

Chen, J.-Y. & Kollmann, W. 1988 PDF Modeling of Chemical Nonequilibrium Effects in Turbulent Nonpremixed Hydrocarbon Flames. *Proceedings of the Twenty-Second Symposium (International) on Combustion.* The Combustion Institute. 645-653.

CHEN, J.-Y. & KOLLMANN, W. 1992 PDF Modeling and Analysis of Thermal NO Formation in Turbulent Nonpremixed Hydrogen-Air Jet Flames. *Combust. Flame.* **88,** 397-412.

CHEN, J.-Y. & KOLLMANN, W. 1994 *Comparison of prediction and measurement in nonpremixed turbulent flames.* in *Turbulent Reacting Flows*, F. A. Williams & P. A. Libby (eds), Academic Press Ltd. 211-308

CORREA, S. M. 1993 Turbulence-Chemistry Interactions in the Intermediate Regime of Premixed Combustion. *Combust. Flame.* **93,** 41-60.

CORREA, S. M., & POPE, S. B. 1992 Comparison of a Monte Carlo PDF/Finite Volume Mean Flow Model with Bluff-Body Raman Data. *Proceedings of the Twenty-Fourth Symposium (International) on Combustion.* The Combustion Institute. 279-285.

DOPAZO, C. 1975 Probability function approach for a turbulent axisymmetric heated jet: centerline evolution. *Phys. Fluids.* **18,** 397.

DOPAZO, C. 1979 On conditioned averages for intermittent turbulent flows. *J. Fluid Mech.* **81,** 433.

FROLOV, S. M. 1996 Private communication.

JANICKA, J., KOLBE W., & KOLLMANN W. 1979 Closure of the transport equation for the probability density of function of scalar fields. *J. Nonequilib. Thermodyn.* **4,** 27.

JANICKA, J., & KOLLMANN, W. 1978 A Two-Variables Formalism for the Treatment of Chemical Reactions in Turbulent H_2-Air Diffusion Flames. *Proceedings of the Seventeenth Symposium (International) on Combustion. The Combustion Institute. 421-430.*

KLIMENKO, A. YU. 1990 Multicomponent diffusion of various admixtures in turbulent flow. *Fluid Dynamics.* **25,** 327-334.

POPE, S. B. 1981 A Monte Carlo Method for the PDF Equations of Turbulent Reactive Flow. *Combust. Sci. Tech.* **25,** 159-174.

POPE, S. B. 1982 An improved turbulent mixing model. *Comb. Sci. Tech.* **28,** 131.

POPE, S. B. 1985 PDF Methods for Turbulent Flows. *Prog. Energy Sci. Comb.* **11,** 119-192.

POPE, S. B. 1990 Computations of Turbulent Combustion: Progress and Challenges. *Proceedings of the Twenty-Third Symposium (International) on Combustion.* The Combustion Institute. 591-612.

SMITH, N. S. A., BILGER, R. W., CARTER, C. D., BARLOW, R. S., & CHEN, J.-Y. 1993 A Comparison of CMC and PDF Modelling Predictions with Experimental Nitric Oxide LIF/Raman Measurements in a Turbulent H_2 Jet Flame. *Combust. Sci. Tech.* **105,** 357-375.

SMITH, N. S. A., BILGER, R. W., CARTER, C. D., BARLOW, R. S., & CHEN J.-Y. 1996 Radiation Effects on Nitric Oxide Formation in Turbulent Hydrogen Jet Flames Diluted with Helium. Submitted to *Combustion and Flame.*